JCTC Journal of Chemical Theory and Computation

Quartic-Scaling Analytical Energy Gradient of Scaled Opposite-Spin Second-Order Møller−Plesset Perturbation Theory

Rohini C. Lochan,[†] Yihan Shao,[§] and Martin Head-Gordon*[,†,‡]

Department of Chemistry, University of California, Berkeley, California 94720, Chemical Sciences Division, Lawrence Berkeley National Laboratory, Berkeley, California 94720 and Q-Chem, Inc., Pittsburgh, Pennsylvania 15213

Received September 21, 2006

Abstract: The analytical gradient of the "scaled opposite spin" (SOS-) and "modified opposite spin" (MOS-) second-order Møller−Plesset perturbation theory (MP2) methods is derived and implemented. Both energy and the first derivative can be evaluated efficiently with a fourth-order scaling algorithm by using a combination of auxiliary basis expansions and Laplace transformation techniques as opposed to the traditional fifth-order approach of MP2. A statistical analysis of 178 small molecules suggests that the new gradient scheme provides geometries of MP2 quality, indicating the reliability of the method in general chemical applications. A more specific study of the group VI transition metal carbonyl complexes indicates that the new scheme improves the MP2 description relative to available experimental data and higher-order theories. The proposed gradient scheme thus endeavors to obtain improved structural features at reduced computational cost.

I. Introduction

One of the key initial steps in any computational study or chemical application is the determination of the equilibrium molecular structure of the constituent systems. The availability of analytical gradients with respect to nuclear displacements for the specific methodology used plays a critical role in the fast and efficient identification of stable geometries or transition states.[1,2] So far, density functional theory (DFT)[3] has remained the most popular choice to obtain optimized molecular geometries in studies that especially involve large molecules, primarily due to its low computational cost and reasonable performance. However, one is constrained to choose the most appropriate functional that is suitable for a particular problem as DFT cannot be improved systematically. Also, the reliability of DFT in studies where long-range dispersive effects are important is questionable, as present-day functionals cannot account for such interactions.[4−8]

On the other hand, ab initio methods like second-order Møller−Plesset perturbation theory (MP2)[9] offer the simplest systematic route to introduce dynamic correlation effects beyond the Hartree−Fock (HF) mean-field approximation[10] and also account for dispersion interactions.[11] However, there are two important considerations that need to be addressed regarding the computational cost and the reliability of MP2 results.

(i) The cost of computing the canonical MP2 energy and analytic gradient grows formally as $\mathcal{O}(M^5)$ with system size, which limits the applicability of MP2 to large molecules. Tremendous effort has gone into developing fast and efficient lower-order scaling MP2 energy[12−25] and gradient codes[26−43] in the past few decades. In particular, the use of the "resolution-of-the-identity" approximation (RIMP2)[12,14,23,40−42] has emerged as an important tool to reduce the computational prefactor of the fifth-order scaling MP2 energy and gradient algorithm, leading to significant speedups at the cost of introducing tolerable error. Then, there are the "local" MP2 (LMP2) approaches that use localized orbitals[13,15,22] or atomic

* Corresponding author e-mail: mhg@cchem.berkeley.edu.
[†] University of California.
[‡] Lawrence Berkeley National Laboratory.
[§] Q-Chem, Inc.

10.1021/ct600292h CCC: $37.00
Published on Web 03/10/2007

truncations[18,23] to obtain low-order scaling MP2 methods to calculate the correlation energy. Some of these methods have been made more efficient by using the RI approximation.[22,23] Analytic gradients are available for a couple of these LMP2 approaches.[35,43] In particular, Schütz et al. have demonstrated that their LMP2 analytic gradient scheme could scale quadratically with system size by exploiting the sparsity of the fit coefficients and employing local domains.[43]

(ii) Although MP2 energies and geometries are known to be quite reliable for closed-shell molecules,[44] they tend to overestimate interaction energies and underestimate bond distances when compared to higher-order theories like coupled-cluster singles and doubles with a perturbative correction method [CCSD(T)][45] or available experimental data. This is particularly true in case of stacking problems, for example, the famous benzene dimer case.[46] This trend is also observed in the prediction of metal−ligand bond dissociation energies and bond lengths in closed-shell transition metal (TM) complexes.[47] When it comes to open-shell systems like radicals and other transition metal compounds, the performance of MP2 is rather poor.[48] Also, MP2 is limited to systems where the single-reference wavefunction-based HF approximation is deemed a good starting point. Finally, approaching the basis set limit of MP2 calculations requires a large basis set description.[49] However, as mentioned earlier, MP2 displays a tendency to overestimate interaction energies, which means that this limit may or may not be more accurate than small basis set results.[46]

Clearly, it is desirable to develop methodologies that are both computationally efficient and accurate. In this context, a family of "scaled" MP2 methods[50−52] was recently proposed, which could achieve significant statistical improvements in performance across various chemical properties and also maintain the size consistency feature of MP2. The idea was first put forth by Grimme,[50] who suggested that separate scaling of the opposite-spin (OS) and same-spin (SS) components of the MP2 correlation energies (SCS-MP2)

$$E_{\mathrm{MP2}} = c_{\mathrm{OS}}E_{\mathrm{OS}} + c_{\mathrm{SS}}E_{\mathrm{SS}} \tag{1}$$

where $c_{\mathrm{OS}} = 6/5$ and $c_{\mathrm{SS}} = 1/3$, could yield QCISD(T) (= quadratic configuration interaction with single and double excitations and triple excitations added perturbatively) quality results as far as relative energies are concerned.[53−57] This method, however, does not offer any computational advantage. Following this, we recently proposed two variants of the above method, where only the OS contribution to the MP2 correlation energy is scaled while the SS contribution is neglected. In the scaled opposite-spin (SOS-MP2) approach,[51] the optimal OS scaling factor that accounts for the absence of the SS contribution was found to be $c_{\mathrm{OS}} = 1.3$. However, for nonoverlapping systems, both SCS-MP2 and SOS-MP2 provide an incorrect physical description of the long-range correlation effects. To correct this deficiency, we then proposed the modified opposite-spin (MOS-MP2)[52] method that instead employs a distance-dependent scaling of the OS correlation energy. The two-electron operator is hence modified to

$$\hat{\Theta}_{\omega}(\mathbf{r}) = \frac{1}{\mathbf{r}} + c_{\mathrm{MOS}}\frac{erf(\omega\mathbf{r})}{\mathbf{r}} \tag{2}$$

where the recommended value for ω is 0.6 au and $c_{\mathrm{MOS}} = (\sqrt{2} - 1)$. Both SOS-MP2 and MOS-MP2 methods (henceforth, collectively known as OS-MP2 methods) are dependent on a single parameter unlike the two-parameter SCS-MP2 approach. In any case, the presence of empirical parameter(s) is a drawback common to all the scaled-MP2 methods as the recommended parameter value might not be suitable for every chemical application. However, in the case of the MOS-MP2 approach, it was found that the parameter ω could be tuned to improve the MP2 performance for a particular property such as barrier height determination.[52] The OS-MP2 methods not only show statistical improvements in accuracy similar to (sometimes even better than) SCS-MP2 but are also computationally advantageous as the inherent fifth-order scaling nature with system size of the traditional MP2 can be reduced to fourth order by using a combination of auxiliary basis expansions[12,14,58] and Laplace transformation,[59] without using any cutoffs.[51,52] Also, by further exploiting the locality and sparsity of the expansion coefficients, the computational cost can be reduced to almost quadratic scaling.[60]

In this work, we derive the analytical gradient of the fourth-order scaling OS-MP2 energy, establish that it can also be evaluated with $\mathcal{O}(M^4)$ computational effort, and validate its chemical and computational performance. This is significant as we can obtain improved results with an inherently low-order scaling MP2-type gradient without using any cutoff schemes, thereby extending the size of systems currently feasible. The analytical gradient equations presented here are exact within the use of RI and Laplace transformation approximations in the OS-MP2 energy expression. The theoretical derivation of the OS-MP2 analytical gradient is presented in section II after a brief review of the standard representations in MP2 gradient theory.

The reported gradient scheme is based on a canonical HF reference (i.e., diagonal Fock matrix), and the final gradient expression is obtained by explicitly differentiating the OS-MP2 energy equation. The fourth-order scaling result is particularly interesting because it would seem to be impossible to obtain if the quartic number of amplitudes must be manipulated explicitly to obtain effective density matrices and two-particle density matrices. However, we show this can be avoided. The proposed algorithm, discussed in section III, can be easily integrated with the existing OS-MP2 energy code and the recently proposed RIMP2 analytic gradient algorithm.[41] The memory requirements for the current implementation remain quadratic, while the cubic disk space needed is doubled when compared to the OS-MP2 energy evaluation. Also, the algorithm is constructed such that it can be easily extended to accommodate the unrestricted cases and the frozen-core approximation.

In section IV, we benchmark the CPU timing performance of the proposed algorithm with a series of linear and globular polyalanine peptide (tetra-, octa-, hexadeca-) systems and compare with the timings obtained by other methods like HF, standard MP2, and RIMP2. We also show that, in

Table 1. Description of the Notation Used in the Derivation

notation	description
$\mu, \nu, \lambda, \sigma$	atomic orbital (AO)
i, j, k, l	active occupied MO
a, b, c, d	active virtual MO
p, q, r, s	any MO
K, L, M, N	auxiliary basis function
τ	Laplace quadrature point[a]
N_τ	number of quadrature points used
n	number of basis functions
o	number of active occupied MOs
v	number of active virtual MOs
N_{aux}	number of auxiliary basis functions
superscript x	derivative with respect to perturbation in the nuclear coordinate x[b]
superscript (x)	derivative of the AO integrals alone (excluding MO coefficients)[c]

[a] Laplace quadrature-dependent terms indicated with left superscript τ, for example, ${}^{\tau}X^{\alpha}_{PQ}$. [b] Example: $S^x_{pq} = \partial S_{pq}/\partial x$ [c] Example: $S^{(x)}_{pq} = \sum_{\mu\nu} C_{\mu p}[(\partial S_{\mu\nu})/(\partial x)]C_{\nu q}$

general, this gradient provides reliable MP2-like geometries for small molecules through a statistical study of 178 systems, and in particular, the OS-MP2 analytical gradient helps to improve the MP2 description of difficult systems like group VI transition metal carbonyls. Finally, in section V, we present some conclusions.

II. Gradient Theory

In this section, we provide a short review of the standard representations of the MP2/RIMP2 analytic gradient and summarize the main energy expressions of the OS-MP2 theory to set the stage for the derivation of the OS-MP2 gradient. Table 1 summarizes the description of the notation/indices used hereafter.

A. Standard Representation of the Analytical MP2 Gradient. The standard representation of the analytical gradient of the conventional MP2 total energy (HF energy + correlation energy) with respect to perturbation in any nuclear coordinate, say x, can be written in the form[61]

$$E^x = \sum_{\mu\nu} P_{\mu\nu} H^x_{\mu\nu} + \sum_{\mu\nu} W_{\mu\nu} S^x_{\mu\nu} + \sum_{\mu\nu\lambda\sigma} \Gamma_{\mu\nu\lambda\sigma} (\mu\nu|\lambda\sigma)^x \quad (3)$$

Here, the gradient is expressed in the atomic orbital (AO) basis as the sum of three pieces, namely, the contraction of one- and two-particle density matrices, $P_{\mu\nu}$ and $\Gamma_{\mu\nu\lambda\sigma}$, with the corresponding derivatives of the one- and two-particle Hamiltonian and, third, the contraction of the energy-weighted density matrix, $W_{\mu\nu}$, with the overlap derivative. The two-particle density matrix (2-PDM) can be written as a sum of a separable and a nonseparable piece[30]

$$\Gamma_{\mu\nu\lambda\sigma} = \Gamma^{S}_{\mu\nu\lambda\sigma} + \Gamma^{NS}_{\mu\nu\lambda\sigma} \quad (4)$$

The separable 2-PDM is given by

$$\Gamma^{S}_{\mu\nu\lambda\sigma} = \frac{1}{2}(P^{HF}_{\mu\nu} + 2P^{(2)}_{\mu\nu})P^{HF}_{\lambda\sigma} - \frac{1}{2}(P^{HF}_{\mu\sigma} + 2P^{(2)}_{\mu\sigma})P^{HF}_{\lambda\nu} \quad (5)$$

The definition of the MP2 correction to the density matrices, $P^{(2)}_{\mu\nu}$, $W^{(2)}_{\mu\nu}$, and $\Gamma^{NS}_{\mu\nu\lambda\sigma}$ is well-known.[30,37,62]

In the case of RIMP2,[12,14] the evaluation of the correlation energy is made computationally faster and efficient by using auxiliary basis expansions to express the four-index integrals in terms of three- and two-center two-electron integrals

$$I_{Coulomb} = (ia|jb) = \sum_K B^K_{ia} B^K_{jb} \quad (6)$$

where

$$B^K_{ia} = \sum_M (ia|M) V^{-1/2}_{MK} \quad (7)$$

and

$$V_{MK} = (M|K) \quad (8)$$

We note that the option of using the RI approximation in HF evaluation is not pursued here. As a consequence of the RI approximation, the three- and two-center two-electron integral derivatives also contribute toward the gradient. Therefore, the analytical gradient of the total RIMP2 energy (HF energy + RIMP2 correlation energy) takes up the form[41,42]

$$E^x_{RI} = \sum_{\mu\nu} P_{\mu\nu} H^x_{\mu\nu} + \sum_{\mu\nu} W_{\mu\nu} S^x_{\mu\nu} + \sum_{\mu\nu\lambda\sigma} \Gamma^{S}_{\mu\nu\lambda\sigma} (\mu\nu|\lambda\sigma)^x + \sum_{\mu\nu}\sum_K \Gamma^K_{\mu\nu} (\mu\nu|K)^x + \sum_{KL} \gamma_{KL} (K|L)^x \quad (9)$$

where, $\Gamma^K_{\mu\nu}$ and γ_{KL} represent the RI-specific 2-PDMs, which are contracted with the three- and two-center two-electron integral derivatives, respectively. The separable 2-PDM retains the same form as eq 5. The explicit definitions of the RIMP2 correction to the density matrices are described elsewhere.[41,42]

B. Review of OS-MP2 Energy Evaluation. Unlike conventional MP2 and RIMP2, the OS-MP2 energy (both SOS- and MOS-MP2) can be evaluated without any fifth-order step when a combination of auxiliary basis functions and a Laplace transformation is applied to the energy expression[51,52]

$$E_{OS} = -\sum_{ia}^{\alpha}\sum_{jb}^{\beta} \frac{\bar{I}^{jb}_{ia}\bar{I}^{jb}_{ia}}{\Delta^{jb}_{ia}} \quad (10)$$

where the energy denominator is given in terms of the canonical orbital energies as $\Delta^{jb}_{ia} = (\epsilon_a - \epsilon_i) + (\epsilon_b - \epsilon_j)$. In the case of SOS-MP2, the integrals $\bar{I}^{jb}_{ia}$ in the above equation are simply the Coulomb integrals given in eq 6, while for MOS-MP2, they are evaluated with the modified two-electron operator $\hat{\Theta}_\omega(\mathbf{r})$ shown in eq 2. The final working expression for computing the OS-MP2 energy can be written as

$$-E_{OS} = \sum_{\tau}^{N_\tau} w_\tau \sum_{KL} {}^{\tau}X^{\alpha}_{KL}\, {}^{\tau}X^{\beta}_{KL} \quad (11)$$

where

$$ {}^{\tau}X^{\alpha}_{KL} = \sum_{ia}^{\alpha} B^{K}_{ia} B^{L}_{ia} ({}^{\tau}\xi^{a}_{i})^{2} \tag{12} $$

and

$$ {}^{\tau}\xi^{a}_{i} = \exp[(\epsilon_{i} - \epsilon_{a}) t_{\tau}/2] \tag{13} $$

The evaluation of the **X** matrix in eq 12 is the dominant step of order $\mathcal{O}(N_{\tau} o v N_{\mathrm{aux}}^{2})$ in the energy evaluation. Notice that the evaluation of the **B** matrix in eq 7 also scales as $\mathcal{O}(M^{4})$ with system size; however, it is independent of the Laplace quadrature and, therefore, evaluated only once in the algorithm.

C. Derivation of the Analytical OS-MP2 Gradient. We now present the formulation of the OS-MP2 analytical gradient, which retains the same standard form expressed in eq 9. However, the explicit definitions of the OS-MP2 correction to the **P**, **W**, Γ, and γ matrices in eq 9 are different from the case of the RIMP2 gradient.[41,42] The formulation presented below is valid for both SOS-MP2 and MOS-MP2 analytical gradients. In the case of the MOS-MP2 gradient, the involved three-center and two-center two-electron integrals and their derivatives are evaluated using the modified two-electron operator given in eq 2. Subsequently, all terms built from these modified integrals would depend on the parameter "ω".[52]

Each piece of the OS-MP2 gradient can be evaluated with $\mathcal{O}(M^{4})$ or lower computational cost, where M is the system size, unlike RIMP2 or MP2 that involve fifth-order scaling terms. This achievement is possible because the quartic number of amplitudes are *never explicitly formed*—instead, all one- and two-particle density matrices are cast in terms of more compact intermediates in the auxiliary basis, such as the **X** matrix defined above in eq 12. For the sake of simplicity, we present the derivation for a restricted closed-shell system. However, the following derivation can be readily extended to the unrestricted case in a straightforward manner.

The OS-MP2 analytical gradient for a restricted, closed-shell system can be obtained by directly differentiating the working energy expression in eq 11, which gives

$$ -\frac{1}{2} E^{x}_{\mathrm{OS}} = \sum_{\tau}^{N_{\tau}} w_{\tau} \sum_{KL} ({}^{\tau}X^{\alpha}_{KL})^{x} {}^{\tau}X^{\beta}_{KL} \tag{14} $$

Straightforward differentiation of eqs 7, 8, 12, and 13 transforms eq 14 to

$$ -\frac{1}{2} E^{x}_{\mathrm{OS}} = \sum_{\tau}^{N_{\tau}} w_{\tau} [\sum_{ia}^{\alpha} \sum_{M} {}^{\tau}\Gamma^{M,\beta}_{ia} ({}^{\tau}\xi^{a}_{i})^{2} \{2(ia|M)^{x} + t_{\tau}(ia|M)(\epsilon^{x}_{i} - \epsilon^{x}_{a})\}] + \sum_{KL} \bar{\gamma}_{KL} V^{x}_{KL} \tag{15} $$

The details about the intermediate steps leading to the above equation are outlined in Appendix A. The three-index RI-specific 2-PDM in the above equation is given by

$$ {}^{\tau}\Gamma^{M,\beta}_{ia} = \sum_{L} {}^{\tau}Y^{\beta}_{ML} B^{L}_{ia} \tag{16} $$

and

$$ {}^{\tau}Y^{\beta}_{ML} = \sum_{K} V^{-1/2}_{MK} {}^{\tau}X^{\beta}_{KL} \tag{17} $$

The formation of the Γ matrix in the eq 16 is the dominant fourth-order step in the evaluation of the analytical gradient and scales as $\mathcal{O}(N_{\tau} o v N_{\mathrm{aux}}^{2})$. Note that this cost is isomorphic with the **X** matrix formation in eq 12. The "Laplace quadrature independent" (indicated by bar above symbol) two-index RI-specific 2-PDM in eq 15 is given by

$$ \bar{\gamma}_{KL} = \sum_{\tau}^{N_{\tau}} w_{\tau} {}^{\tau}\gamma_{KL} \tag{18} $$

and

$$ {}^{\tau}\gamma_{KL} = -\sum_{M} {}^{\tau}Y^{\alpha}_{KM} {}^{\tau}Y^{\beta}_{ML} \tag{19} $$

In eq 15, the three-center, two-electron integral derivative is given by

$$ (ia|M)^{x} = (ia|M)^{(x)} + \sum_{p} U^{x}_{pi}(pa|M) + \sum_{p} U^{x}_{pa}(ip|M) \tag{20} $$

where

$$ (ia|M)^{(x)} = \sum_{\mu\nu} C_{\mu i} (\mu\nu|M)^{x} C_{\nu a} \tag{21} $$

The terms U^{x}_{pi} and U^{x}_{pa} in eq 20 represent the orbital responses to the displacement x. Rewriting the first term in eq 15 by inserting eq 20 gives

$$ 2 \sum_{\tau}^{N_{\tau}} w_{\tau} \sum_{ia}^{\alpha} \sum_{M} {}^{\tau}\Gamma^{M,\beta}_{ia} ({}^{\tau}\xi^{a}_{i})^{2} (ia|M)^{x} = 2 \sum_{M} [\sum_{\mu\nu} \bar{\Gamma}^{M,\beta}_{\mu\nu} (\mu\nu|M)^{x} + \sum_{\tau}^{N_{\tau}} w_{\tau} \sum_{ia}^{\alpha} {}^{\tau}\Gamma^{M,\beta}_{ia} ({}^{\tau}\xi^{a}_{i})^{2} \sum_{p}^{\mathrm{all}} \{(pa|M) U^{x}_{pi} + (ip|M) U^{x}_{pa}\}] \tag{22} $$

In the above equation, the first term is obtained by scaling and incrementing the Γ matrix in the molecular orbital (MO) basis for every Laplace quadrature point, τ, to produce a "Laplace quadrature independent" quantity

$$ \bar{\Gamma}^{M,\beta}_{ia} = \sum_{\tau}^{N_{\tau}} w_{\tau} {}^{\tau}\Gamma^{M,\beta}_{ia} ({}^{\tau}\xi^{a}_{i})^{2} \tag{23} $$

Subsequently, the $\bar{\Gamma}$ matrix is back-transformed into the AO basis by rearranging the MO coefficients in eq 21 through two fourth-order scaling steps of order $\mathcal{O}(o v n N_{\mathrm{aux}} + o n^{2} N_{\mathrm{aux}})$

$$ \bar{\Gamma}^{M,\beta}_{\mu\nu} = \sum_{i}^{\alpha} C_{\mu i} (\sum_{a}^{\alpha} C_{\nu a} \bar{\Gamma}^{M,\beta}_{ia}) \tag{24} $$

Note that the two-step back-transformation has to be performed only once as the Laplace quadrature independent $\bar{\Gamma}$ matrix is used in eq 24.

The second and third terms in eq 22 involve the occupied−occupied, occupied−virtual, virtual−occupied, and virtual−

virtual blocks of the orbital response matrix, U^x. Following the strategies used by Aikens et al.,[37] we make use of the closed-shell coupled-perturbed Hartree−Fock equations (see Appendix B) and the orthonormality constraint

$$U^x_{pq} + U^x_{qp} + S^x_{pq} = 0 \tag{25}$$

to manipulate the sum of the second term in eq 22 and the second term in eq 15 through some interesting algebra (see Appendix C) to arrive at

$$2\sum_{\tau}^{N_\tau} w_\tau \sum_{ia}^{\alpha}\sum_{M}\{\sum_{p}^{\text{all}} (pa|M)U^x_{pi} + t_\tau(ia|M)\epsilon^x_i\}{}^{\tau}\Gamma^{M,\beta}_{ia}({}^{\tau}\xi^a_i)^2 = \sum_{ki}^{\alpha}\bar{P}^{(2)}_{ki}\left(\frac{Q^x_{ki}+Q^x_{ik}}{2}\right) + 2\sum_{ci}^{\alpha}\overline{(L1)}_{ci}U^x_{ci} - \sum_{ki}^{\alpha}\overline{(L1)}_{ki}S^x_{ki} \tag{26}$$

where

$$\bar{P}^{(2)}_{ki} = \sum_{\tau}^{N_\tau} w_\tau\, {}^{\tau}g_{ki}(z)\, {}^{\tau}\Omega_{ki} \tag{27}$$

and

$${}^{\tau}\Omega_{ki} = \sum_{a}^{\alpha}({}^{\tau}\xi^a)^2\sum_{M}(ka|M)\,{}^{\tau}\Gamma^{M,\beta}_{ia} \tag{28}$$

and

$${}^{\tau}g_{ki} = \frac{{}^{\tau}\xi_k{}^2 - {}^{\tau}\xi_i{}^2}{\epsilon_k - \epsilon_i} = t_\tau \exp[(\epsilon_k+\epsilon_i)t_\tau/2]\frac{\sinh[(\epsilon_k-\epsilon_i)t_\tau/2]}{[(\epsilon_k-\epsilon_i)t_\tau/2]} \tag{29}$$

and

$$\overline{(L1)}_{pi} = \sum_{\tau}^{N_\tau} w_\tau \sum_{a}^{\alpha}({}^{\tau}\xi^a_i)^2\sum_{M}{}^{\tau}\Gamma^{M,\beta}_{ia}(pa|M) \tag{30}$$

The expressions for Q^x_{ki} are given by eqs B1 and B2. In the above equations, ${}^{\tau}\xi_i = \exp(\epsilon_i t_\tau/2)$ and ${}^{\tau}\xi^a = \exp(-\epsilon_a t_\tau/2)$. The details of the steps involved in arriving at eq 26 are indicated in Appendix C.

Similarly, the sum of the third terms in eqs 15 and 22 can be written as

$$2\sum_{\tau}^{N_\tau} w_\tau \sum_{ia}^{\alpha}\sum_{M}\{\sum_{p}^{\text{all}} (ip|M)U^x_{pa} - t_\tau(ia|M)\epsilon^x_a\}{}^{\tau}\Gamma^{M,\beta}_{ia}({}^{\tau}\xi^a_i)^2 = \sum_{ca}^{\alpha}\bar{P}^{(2)}_{ca}\left(\frac{Q^x_{ca}+Q^x_{ac}}{2}\right) + 2\sum_{ka}^{\alpha}\overline{(L2)}_{\text{ka}}U^x_{ka} - \sum_{ca}^{\alpha}\overline{(L2)}_{ca}S^x_{ca} \tag{31}$$

where

$$\bar{P}^{(2)}_{ca} = \sum_{\tau}^{N_\tau} w_\tau\, {}^{\tau}g_{ca}\, {}^{\tau}\Omega_{ca} \tag{32}$$

and

$${}^{\tau}\Omega_{ca} = \sum_{i}^{\alpha}({}^{\tau}\xi_i)^2\sum_{M}(ic|M)\,{}^{\tau}\Gamma^{M,\beta}_{ia} \tag{33}$$

and

$${}^{\tau}g_{ca} = \frac{{}^{\tau}\xi_c{}^2 - {}^{\tau}\xi_a{}^2}{\epsilon_c - \epsilon_a} = -t_\tau \exp[-(\epsilon_c+\epsilon_a)t_\tau/2]\frac{\sinh[-(\epsilon_c-\epsilon_a)t_\tau/2]}{[-(\epsilon_c-\epsilon_a)t_\tau/2]} \tag{34}$$

and

$$\overline{(L2)}_{pa} = \sum_{\tau}^{N_\tau} w_\tau \sum_{i}^{\alpha}({}^{\tau}\xi^a_i)^2\sum_{M}{}^{\tau}\Gamma^{M,\beta}_{ia}(ip|M) \tag{35}$$

The "g" function introduced in eqs 29 and 34 above is continuous at the limit of $\epsilon_i \approx \epsilon_k$ (or $\epsilon_c \approx \epsilon_a$) and tends to the finite value $t_\tau({}^{\tau}\xi_i)^2$ [or $-t_\tau({}^{\tau}\xi^a)^2$]. It thus ensures that the first term in eqs 26 and 31 are well-behaved when nearly degenerate orbitals are encountered.[25]

When all of the information given above is used, the expression of the analytical gradient of the closed-shell OS-MP2 energy takes up the form

$$-\frac{1}{2}E^x_{\text{OS}} = \sum_{ik}^{\alpha}\bar{P}^{(2)}_{ki}\left(\frac{Q^x_{ki}+Q^x_{ik}}{2}\right) + \sum_{ik}^{\alpha}\overline{(L1)}_{ki}S^x_{ki} + \sum_{ca}^{\alpha}\bar{P}^{(2)}_{ca}\left(\frac{Q^x_{ca}+Q^x_{ac}}{2}\right) + \sum_{ca}^{\alpha}\overline{(L2)}_{ca}S^x_{ca} + 2\sum_{ck}^{\alpha}\overline{(L1)}_{ck}U^x_{ck} + 2\sum_{kc}^{\alpha}\overline{(L2)}_{kc}U^x_{kc} + 2\sum_{\mu\nu}\sum_{M}\bar{\Gamma}^{M,\beta}_{\mu\nu}(\mu\nu|M)^x + \sum_{KL}\bar{\gamma}_{KL}V^x_{KL} \tag{36}$$

From this stage on, the expression for the OS-MP2 analytical gradient takes up the same form as the corresponding RIMP2 analytical gradient expression.[41] Although further manipulation is required to arrive at the final standard expression given in eq 9, it involves the same strategies and techniques that were used in the derivation of the RIMP2 analytical gradient and will not be discussed in detail here. Some of the important steps following eq 36 are the assembly of the Lagrangian, followed by the iterative solution of the **Z**-vector equation[27] to obtain the virtual−occupied block of the 1-PDM, **P**, and finally, with the help of eqs B4−B6 and further rearrangements, the standard expression given in eq 9 can be obtained.[37,41] The final expressions of the energy-weighted 1-PDM, $\bar{\mathbf{W}}$ is summarized below:

$$\text{occ−occ:}\ \ \bar{\mathbf{W}}_{ki} = -\overline{(L1)}_{ki} - \frac{1}{2}(\epsilon_i+\epsilon_k)\bar{P}_{ki} - \frac{1}{2}\sum_{pq}A_{pqki}\bar{P}_{pq} \tag{37}$$

$$\text{occ−vir:}\ \ \bar{\mathbf{W}}_{kc} = -\overline{(L2)}_{kc} \tag{38}$$

$$\text{vir−occ:}\ \ \bar{\mathbf{W}}_{ck} = -\frac{1}{2}\epsilon_k\bar{P}_{ck} \tag{39}$$

$$\text{vir−vir:}\ \ \bar{\mathbf{W}}_{ca} = -\overline{(L1)}_{ca} - \frac{1}{2}\epsilon_a\bar{P}_{ca} \tag{40}$$

The effective Lagrangian L_{ck} that goes into the **Z**-vector equation, eq B9, is given by

$$\bar{L}_{ck} = \overline{(L1)}_{ck} + \overline{(L2)}_{ck} + \overline{(L3)}_{ck} \tag{41}$$

and

$$(\overline{L3})_{ck} = \sum_{ij} A_{ijck}\bar{P}_{ij} + \sum_{ab} A_{abck}\bar{P}_{ab} \qquad (42)$$

$(\overline{L1})_{ai}$ and $(\overline{L2})_{ai}$ in eq 41 are defined by eqs 30 and 35, respectively.

III. Fourth-Order Scaling Algorithm

In this section, we present the algorithmic details of the efficient fourth-order implementation of the proposed gradient method beyond the initial self-consistent field (SCF) steps. It is convenient to break up the post-SCF algorithm into the following four major sections.

A. Pre-Gradient. This section of the algorithm prepares for the evaluation of OS-MP2 energy and analytical gradient as shown in Chart 1. Similar to the OS-MP2 energy algorithm,[51,52] the first two steps involve the formation of $V_{KL}^{-1/2}$ and $(ia|K)$, which are subsequently used to form B_{ia}^{L} through a simple matrix multiplication. Following this step, the three-center two-electron integrals are transposed to the order (a, i, K) going in the order of the fastest to the slowest index and stored on disk in order to efficiently form the 1-PDM contributions in the next stage of the algorithm.

B. Gradient I. This part of the algorithm involves the formation of the Laplace dependent quantities. The major steps are outlined in Chart 2. It includes the formation of the **X** and the 2-PDM, ${}^{\tau}\Gamma$ matrix, for each Laplace quadrature point through two almost isomorphic fourth-order scaling steps, which are incidentally the dominant fourth-order steps of the OS-MP2 energy and gradient evaluation. The contributions to the occupied−occupied and virtual−virtual blocks of the 1-PDM, **P**, are also obtained through the formation of intermediate matrices that involve two smaller fourth-order steps. The matrices, ${}^{\tau}\gamma$, ${}^{\tau}\Gamma$, and **P** are then appropriately scaled and incremented on disk in order to form the Laplace quadrature independent quantities that will be used in the next part of the algorithm.

C. Gradient II. The RI-specific gradient entities are formed in this section. In particular, some of the small fourth-order scaling steps involved in this section are the formation of the pieces of the Lagrangian, **L1** and **L2**, the two-step back-transformation of the $\bar{\Gamma}$ from a MO to AO basis, and finally contribution to the OS-MP2 gradient is obtained by contracting the three-index RI-specific 2-PDM, $\bar{\Gamma}$, with the corresponding three-center integral derivatives. Also, the analogous contribution to the gradient from the two-index RI-specific 2-PDM $\bar{\gamma}$ contracted with the two-center integral derivatives is accumulated. The outline of the major steps is shown in Chart 3.

D. Gradient III. The final section of the algorithm wraps up the evaluation of the analytical gradient. The last piece of the Lagrangian, **L3**, which is a Fock-like matrix given by eq 41, is formed. It has a quartic computational cost for small systems and a quadratic cost for large systems.[36] With the assembly of the effective Lagrangian, the **Z**-vector equation[27] can be solved self-consistently analogous to the SCF iterations, to obtain the virtual−occupied block of the 1-PDM, **P**. Finally, the 1-PDM, **P**; energy-weighted 1-PDM, **W**; and the separable 2-PDM, Γ^{S} are assembled, and the corresponding contributions to the overall gradient are obtained by the contraction with the respective nuclear derivatives.

Chart 1. The Major Steps of the *Pregradient* Algorithmic Section along with the Details of the Ordering of Indices of the Various Entities Involved[a]

	Index order	CPU	Disk
Form $V_{KL}^{-1/2}$	$\forall\, K,L$	N_{aux}^{3}	N_{aux}^{2}
Make $I_{ia}^{K} = (ia\|K)$	$\forall\, a,K,i$	$n^2vN_{aux} + novN_{aux}$	ovN_{aux}
Transpose I_{ia}^{K}	$\forall\, a,i,K$		ovN_{aux}
$B_{ia}^{K} = \sum_{M} (ia\|M) V_{MK}^{-1/2}$	$\forall\, a,K,i$	ovN_{aux}^{2}	ovN_{aux}

[a] Cost of computation and order of disk storage, if necessary, are shown below.

Chart 2. The Major Steps of the *Gradient I* Algorithmic Section along with the Details of the Ordering of Indices of the Various Entities Involved[a]

	Index order	CPU	Disk
Loop over quadrature points, τ			
Loop over i			
Read B_{ia}^{K}	$\forall\, a,K,$ given i		
${}^{\tau}X_{KL}^{\alpha} += \sum_{a}^{\alpha} B_{ia}^{K} B_{ia}^{L}$		$N_\tau \cdot ovN_{aux}^{2}$	
$E_{SOS-MP2} -= \sum_{\tau}^{N_\tau} w_\tau \sum_{KL} {}^{\tau}X_{KL}^{\alpha}\, {}^{\tau}X_{KL}^{\beta}$		$N_\tau \cdot N_{aux}^{2}$	
Read $V_{MK}^{-1/2}$	$\forall\, M,K$		
${}^{\tau}Y_{ML}^{\beta} = \sum_{K} V_{MK}^{-1/2}\, {}^{\tau}X_{KL}^{\beta}$		$N_\tau \cdot N_{aux}^{3}$	
$\bar{\gamma}_{KL} -= \sum_{\tau}^{N_\tau} w_\tau \sum_{M} {}^{\tau}Y_{KM}^{\alpha}\, {}^{\tau}Y_{ML}^{\beta}$		$N_\tau \cdot N_{aux}^{3}$	N_{aux}^{2}
Loop over i			
Read B_{ia}^{L}	$\forall\, a,L,$ given i		
${}^{\tau}\Gamma_{ia}^{M,\beta} = \sum_{L} {}^{\tau}Y_{ML}^{\beta} B_{ia}^{L}$		$N_\tau \cdot ovN_{aux}^{2}$	ovN_{aux}
Loop over M batches (batch size P)			
Read I_{ka}^{M}	$\forall\, a,k,M \in P$		
Transpose I_{ka}^{M}	$\forall\, k,a,M \in P$		
Loop over i			
Read ${}^{\tau}\Gamma_{ia}^{M,\beta}$	$\forall\, a,M \in P,$ given i		
Accumulate ${}^{\tau}\Gamma_{ia}^{M,\beta}$	$\forall\, a,M \in P, \forall\, i$		
${}^{\tau}\Omega_{ki} += \sum_{a}^{\alpha} I_{ka}^{M}\, {}^{\tau}\Gamma_{ia}^{M,\beta} \left({}^{\tau}\xi_{i}^{\alpha}\right)^{2}$		$N_\tau \cdot o^2vN_{aux}$	
$\bar{\Gamma}_{ia}^{M,\beta} += \sum_{\tau}^{N_\tau} w_\tau\, {}^{\tau}\Gamma_{ia}^{M,\beta} \left({}^{\tau}\xi_{i}^{\alpha}\right)^{2}$	$\forall\, a,i,M \in P$		ovN_{aux}
Loop over M batches (batch size P)			
Read I_{ic}^{M}	$\forall$ c,$i,M \in P$		
Loop over i			
Read ${}^{\tau}\Gamma_{ia}^{M,\beta}$	$\forall$ a,$M \in P,$ given i		
Accumulate ${}^{\tau}\Gamma_{ia}^{M,\beta}$	$\forall\, i,M \in P, \forall a$		
${}^{\tau}\Omega_{ca} += \sum_{i}^{\alpha} I_{ic}^{M}\, {}^{\tau}\Gamma_{ia}^{M,\beta} \left({}^{\tau}\xi_{i}\right)^{2}$		$N_\tau \cdot ov^2N_{aux}$	
$\bar{P}_{ki} += \sum_{\tau}^{N_\tau} w_\tau\, {}^{\tau}\Omega_{ki}\, {}^{\tau}g_{ki}$			o^2
$\bar{P}_{ca} += \sum_{\tau}^{N_\tau} w_\tau\, {}^{\tau}\Omega_{ca}\, {}^{\tau}g_{ca}$			v^2
End loop over quadrature points, τ			

[a] Cost of computation and order of disk storage, if necessary, are shown below.

Of the four major sections described above, in terms of algorithm and coding, only *Gradient I* is unique to the evaluation of the OS-MP2 gradient. The existing OS-MP2 energy code can be readily extended to evaluate key entities like ${}^{\tau}\Gamma$ and **P**. The section *Gradient II* is common between RIMP2 and OS-MP2 gradient schemes,[41] while the final section, *Gradient III*, is common for all MP2-based analytical gradient evaluations.[36,41] We will therefore concentrate on only discussing the algorithmic details of *Gradient I* and refer the reader to refs 36 and 41 for further information on the other sections of the algorithm. Also, the changes that are

Chart 3. The Major Steps of the *Gradient II* Algorithmic Section along with the Details of the Ordering of Indices of the Various Entities Involved[a]

	Index order	CPU	Disk
Loop over M batches (batch size P)			
Read $\bar{\Gamma}_{ia}^{M,\beta}$	$\forall a,i,M \in P$		
Back-transform: $\bar{\Gamma}_{i\nu}^{M,\beta} \leftarrow \bar{\Gamma}_{ia}^{M,\beta}$	$\forall \nu,\mathrm{i},M \in P$	$novN_{aux}$	noN_{aux}
Loop over M batches (batch size P)			
Read $\bar{\Gamma}_{i\nu}^{M,\beta}$	$\forall \nu,i,M \in P$		
Transpose $\bar{\Gamma}_{i\nu}^{M,\beta}$	$\forall i,M \in P,\forall \nu$		
Make $(\mu\nu\|M)$	$M \in P,\forall \mu,\nu$	n^2N_{aux}	
$(\overline{L2})_{i\nu} += \sum_{\nu M} \bar{\Gamma}_{i\nu}^{M,\beta}(\mu\nu\|M)$	$\forall i,\nu$	n^2oN_{aux}	no
Transform $(\mu\nu\|M) \rightarrow (i\nu\|M)$	$M \in P,\forall \nu,i$	n^2oN_{aux}	
Read $\bar{\Gamma}_{ia}^{M,\beta}$	$\forall a,i,M \in P$		
$(\overline{L1})_{a\nu} += \sum_{iM} \bar{\Gamma}_{ia}^{M,\beta}(i\nu\|M)$	$\forall a,\nu$	$novN_{aux}$	nv
Loop over M batches (batch size P)			
Read $\bar{\Gamma}_{i\nu}^{M,\beta}$	$\forall \nu,i,M \in P$		
Transpose $\bar{\Gamma}_{i\nu}^{M,\beta}$	$M \in P,\forall \nu,i$		
Make $(\mu\nu\|M)^x$	$M \in P,\forall \nu,\mu$	n^2N_{aux}	
$E^x += \sum \bar{\Gamma}_{\mu\nu}^{M,\beta}(\mu\nu\|M)^x$		n^2N_{aux}	
Read $\bar{\gamma}_{KL}$	$\forall K,L$		
Make $(K\|L)^x$	$\forall K,L$	N_{aux}^2	
$E^x += \sum \bar{\gamma}_{KL}(K\|L)^x$			

[a] Cost of computation and order of disk storage, if necessary, are shown below.

required to incorporate frozen-core approximation need to be made only in the *Gradient II* and *Gradient III* sections. As this is already implemented,[36,41] the OS-MP2 gradient can automatically and conveniently deal with the frozen-core approximation with no further changes.

At this stage, we would also like to note that, between SOS-MP2 and MOS-MP2 analytical gradient implementations, the only major difference is the use of modified three- and two-index two-electron integrals, $\bar{I}(\omega) = I_{\mathrm{Coulomb}} + c_{\mathrm{MOS}} \cdot I_{\mathrm{Erf}}(\omega)$, and integral derivatives, $\bar{I}^x(\omega) = I^x_{\mathrm{Coulomb}} + c_{\mathrm{MOS}} \cdot I^x_{\mathrm{Erf}}(\omega)$, in the latter algorithm, which is obtained at almost no additional cost.[52] Therefore, all algorithmic discussion of the SOS-MP2 gradient is applicable to the MOS-MP2 analytical gradient as well.

In this implementation of the OS-MP2 analytical gradient, we endeavor to achieve fourth-order CPU scaling, quadratic memory ($\sim 3N_{\mathrm{aux}}^2$), cubic disk storage ($\sim 4ovN_{\mathrm{aux}}$), and third-order I/O. In both RIMP2[41] and the OS-MP2 gradient, the formation of the three-index 2-PDM is the dominating step with costs $\mathcal{O}(o^2v^2N_{\mathrm{aux}})$ and $\mathcal{O}(N_\tau ovN_{\mathrm{aux}}^2)$, respectively. Similar to the discussion on the evaluation of the RIMP2 and OS-MP2 energy, there is a contest between the inherent fifth-order nature of the former and the repeated evaluation of the dominating fourth-order step for each Laplace quadrature point for the latter. However, as the system size increases, the fourth-order nature of the OS-MP2 analytical gradient would eventually kick in and considerable improvements in the CPU timing would be seen. This aspect will be discussed further in the Results and Discussion section. There are a few other competing fourth-order steps in the OS-MP2 gradient evaluation that would tend to dominate the calculation, especially for small systems. For instance, the iterative **Z**-vector solution and final assembly of **P**, **W**, and Γ^{S} are isomorphic with the SCF and SCF gradient evaluations. However, these are also highly dependent on the cutoff employed for integral thresholding and convergence criterion, as we will see in the next section.

The evaluation of the analytical gradient is done mainly through a series of matrix multiplications. The upper bound on the memory requirement for these matrix multiplications is $\mathcal{O}(3N_{\mathrm{aux}}^2)$, which is required to form, for example, eq 17. We should note here that the evaluation of the OS-MP2 energy also has the same memory requirement. In order to maintain this requirement, the three index entities are saved on disk and read, when necessary, within a loop structure that only requires quadratic memory to perform the matrix multiplication. Also, the three-index quantities are saved to disk in an order that would avoid disk-based sorting and unnecessary transpositions. For example, the three-index 2-PDM, ${}^\tau\Gamma$, is initially formed in the order (a, P, i), moving from the fastest to the slowest index, which is then used in eqs 28 and 33 to form the intermediate ${}^\tau\Omega_{ki}$ and ${}^\tau\Omega_{ca}$ matrices. They are, however, subsequently transposed, incremented, and saved to the disk in the order (a, i, P) in order to reduce the number of read and seek operations on disk, when they are later used to form the **L1** and **L2** matrices in the *Gradient II* section.

In the formation of the intermediates, ${}^\tau\Omega_{ki}$ and ${}^\tau\Omega_{ca}$, through eqs 28 and 33, looping over the free indices k and i (or c and a, respectively) leads to a fourth-order I/O step. In order to avoid this, the intermediates are efficiently formed through a batching scheme over the auxiliary basis functions. For example, to form ${}^\tau\Omega_{ki}$ through eq 28, $(ka|M)$ and ${}^\tau\Gamma_{ia}^{M,\beta}$ are loaded as tiles of size ovP from disk to memory, where the batch size, P, is determined by the memory constraint discussed above, giving $P = (3N_{\mathrm{aux}}^2 - o^2)/(2ov + v)$. The tiles of integrals $(ka|M)$ that are read in order (a, k, $M \in P$) are subsequently transposed in memory to the order (k, a, $M \in P$), while the tile ${}^\tau\Gamma_{ia}^{M,\beta}$ is accumulated in the order (a, $M \in P$, i). A smaller batch size, $P = (3N_{\mathrm{aux}}^2 - v^2)/(2ov + v)$, is used for the formation of ${}^\tau\Omega_{ca}$.

Apart from a small number of quadratic entities, the major disk storage corresponds to the three-index quantities of size ovN_{aux}. At first glance, the current gradient scheme might seem to require about $6ovN_{\mathrm{aux}}$ disk space. This can be reduced to just $4ovN_{\mathrm{aux}}$ by overwriting files holding intermediate quantities like ${}^\tau\Gamma_{ia}^{M,\beta}$ and $\bar{\Gamma}_{i\nu}^{M,\beta}$. In comparison to the energy calculation, the amount of disk space required to do a gradient evaluation is almost doubled. This is a modest increase. For example, to do an OS-MP2 analytical gradient calculation on a hexadeca alanine peptide with a 6-31G* basis and a double-ζ quality auxiliary basis ($o = 225$; $v = 1305$; $N_{\mathrm{aux}} = 5390$; $n = 1610$) would imply a disk storage requirement of $\sim$50 GB.

IV. Results and Discussion

In this section we evaluate the performance of the proposed method both computationally and chemically. We have implemented the quartic scaling SOS-MP2 and MOS-MP2 analytical gradient schemes in our quantum chemical software package, QCHEM 3.0.[63] All reported calculations were performed with QCHEM. While the discussion above

Table 2. CPU Timings Obtained on Opteron Cluster for the Force Evaluation of Polyalanine Peptides with 6-31G** Basis and the Corresponding Auxiliary Basis at Various Levels of Theory (in Seconds)

		full gradient CPU timing[a]				
system[b]	SCF	HF[c]	MP2	RIMP2	SOS-MP2	MOS-MP2
			3D			
Tetra	1153	1704	9160	4470	4106	4141
Octa	6773	9596	121 473	46 953	30 513	30 853
HexaDeca	32 751	46 305		781 151	226 751	227 251
			1D			
Tetra	847	1253	6559	3400	3010	3046
Octa	3909	5672	68 989	34 389	18 459	18 689
HexaDeca	20 379	29 098		721 879	166 379	164 979

[a] Full gradient CPU timing = SCF + correlation energy + gradient. [b] Number of basis functions (n): $n_{\text{Tetra}} = 410$; $n_{\text{Octa}} = 810$; $n_{\text{HexaDeca}} = 1610$. [c] HF energy + gradient timing.

referred to the algorithm for a closed-shell case, we have also implemented the straightforward extensions necessary to perform unrestricted calculations and to use the frozen-core approximation.

A. Benchmark Timing. We have considered linear (1D) and globular (3D) polyalanine peptides (tetra-, octa-, and hexadeca-) as model systems to benchmark the computational performance of the proposed algorithm. Table 2 reports the total CPU benchmark timings obtained for the analytical force evaluation of the above systems on a 2 GHz AMD Opteron processor with a 1 GB memory limit using the 6-31G** basis with frozen-core approximation and a double-ζ valence polarized auxiliary basis set. A threshold of 10^{-12} au was employed for integral screening, while the SCF direct inversion in the iterative space (DIIS) convergence was set to 10^{-8} au for all calculations unless specified otherwise.

Table 2 clearly indicates that the use of auxiliary basis expansions brings about significant speedups in the gradient evaluation. For example, if we consider the tetrapeptides, the RIMP2 gradient evaluation is about twice as fast as the conventional MP2 gradient and costs less than 3 times that of the HF gradient. On the other hand, the SOS-MP2 and MOS-MP2 gradient timings are slightly lower than the corresponding RIMP2 timings. The similarity in timings reflects the contest between the repeated evaluation of the fourth-order scaling steps for each Laplace quadrature point in the OS-MP2 methods and the fifth-order scaling steps of RIMP2 for small systems. Also, it indicates that the crossover occurs around the 20 heavy atom regime (less than 400 basis functions) for these polypeptide systems. The SOS-MP2 and MOS-MP2 gradient timings are very similar for all systems considered, indicating that the extra cost of evaluating the modified long-range integrals and their first derivatives for the latter method is almost negligible.

As the system size increases, the fourth-order scaling behavior of the OS-MP2 analytical gradient becomes more apparent. At the octapeptide level, the OS-MP2 gradient costs about 3 times the HF gradient and is about 4 times faster than the conventional MP2 gradient. At the hexadeca level (80 heavy atom regime and about 1610 basis functions), the OS-MP2 gradient timings show significant speedups and are about 4 times faster than the corresponding RIMP2 timings. Table 2 also indicates that dimensionality of the system is critical to the overall CPU timing. Globular systems are more expensive than the linear analogues due to the larger number of significant AO basis function pairs.

In order to take a closer look at the performance of the method, Tables 3 and 4 show the CPU timings obtained for the key steps of the SOS-MP2 energy and gradient calculation for the linear and globular polypeptides. The formation of the $\mathbf{X}$ matrix and $\bar{\Gamma}$ matrix, solution of the $\mathbf{Z}$-vector equation, and assembly of the separable part of the 2-PDM (Γ^{S}) are among the most time-consuming steps in the evaluation of the analytical SOS-MP2 gradient. The costs of evaluating $\mathbf{X}$ and $\bar{\Gamma}$ are isomorphic given that both terms go as $\mathcal{O}(N_{\tau o \upsilon} N_{\text{aux}}^{2})$. The latter is slightly more expensive due to the additional cost of incrementing the 2-PDM on disk for each Laplace quadrature point and becomes the dominant fourth-order step in the evaluation of the SOS-MP2 analytical gradient as the system size increases. For small systems, the solution of the $\mathbf{Z}$-vector equation and formation of the Γ^{S} matrix dominate the gradient calculation. However, these two steps [and also the formation of $(ia|P)$, other pieces of *Gradient II* and *Gradient III*] are inextricably connected to the dimensionality of the system and the cutoff for the integral screening. With a tight integral cutoff (10^{-12} au), these two steps, therefore, appear to dominate the calculation for a large system like the globular hexadecapeptide. The corresponding linear analogue clearly indicates that the $\mathbf{X}$ and $\bar{\Gamma}$ formation becomes the most time-consuming step. In order to emphasize the effect of the integral threshold, the timings obtained for a looser cutoff (integral threshold: 10^{-10} au; DIIS convergence: 10^{-7}) are also shown in Tables 3 and 4. The looser criteria thus enable us to speed up the SCF, SCF Gradient, and Gradient III calculations by about 40%, 38%, and 27% for the globular hexadecapeptides and by about 38%, 30%, and 24% for the linear analogue, respectively. We should note here that the choice of threshold is closely related to the accuracy of the calculation. Tight tolerances are recommended if a high level of accuracy is desired. On the other hand, the various pieces of the energy [excluding $(ia|P)$ formation] and *Gradient I* evaluation are independent of the cutoff threshold as well as dimensionality of the system and, therefore, show no change in computational cost between the linear and globular analogues. We should also emphasize at this stage that the speedups obtained by the SOS-MP2 and MOS-MP2 analytical gradient lies

Table 3. Breakdown of the Dominant Fourth-Order CPU Steps in the SOS-MP2 Energy and Force/Gradient Evaluation of the Globular/Three-Dimensional Polyalanine Peptides with 6-31G** Basis and Its Corresponding Auxiliary Basis (in Seconds)

		tetra.3D		octa.3D		hexadeca.3D	
	criterion[a]	8/12	7/10	8/12	7/10	8/12	7/10
SCF		1153	717	6773	3991	32 751	19 601
HF gradient		550	353	2823	1725	13 553	8191
CPU	energy + gradient[b]	2953	2463	23 740	19 710	194 000	168 500
energy	$(ia\|P)$	44	41	486	425	5987	5214
	B_{ia}^{Q}	22	23	326	325	4943	4957
	X_{PQ}	150	151	2222	2221	33 870	33 990
Gradient I	$\bar{\Gamma}_{ia}^{P}$	164	167	2363	2358	35 247	35 343
	${}^{\tau}\Omega_{ki}$	24	26	303	304	2584	2538
	${}^{\tau}\Omega_{ca}$	50	49	643	649	9152	9144
Gradient II	$(\overline{L1})_{iv} + (\overline{L2})_{av}$	73	67	724	674	7889	6887
	$\sum_{\mu\nu M}(\mu\nu\|M)\bar{\Gamma}_{\mu\nu}^{M,\beta}$	80	73	620	517	5185	4546
Gradient III	$(\overline{L3})$	270	209	1747	1284	9279	6694
	Z vector	926	724	6099	4503	32 940	23 780
	$\Gamma_{\mu\nu\lambda\sigma}^{S}$	1084	867	7651	5898	41 880	30 490

[a] Cutoff for integral thresholding/SCF covergence criterion. [b] CPU timing = correlation energy + SOS-MP2 gradient.

Table 4. Breakdown of the Dominant Fourth-Order CPU Steps in the SOS-MP2 Energy and Force/Gradient Evaluation of the Linear/One-Dimensional Polyalanine Peptides with 6-31G** Basis and Its Corresponding Auxiliary Basis (in Seconds)

		tetra.1D		octa.1D		hexadeca.1D	
	criterion[a]	8/12	7/10	8/12	7/10	8/12	7/10
SCF		847	554	3909	2476	20 379	12 493
HF gradient		406	296	1763	1246	8719	5788
CPU	energy + gradient[b]	2163	1849	14550	13 230	146 000	135 000
energy	$(ia\|P)$	36	34	337	311	4671	4466
	B_{ia}^{Q}	23	23	322	326	4932	4942
	X_{PQ}	150	150	2218	2220	33 880	33 890
Gradient I	$\bar{\Gamma}_{ia}^{P}$	164	154	2350	2366	35 319	35 345
	${}^{\tau}\Omega_{ki}$	24	24	289	303	2582	2577
	${}^{\tau}\Omega_{ca}$	49	49	634	647	9168	9173
Gradient II	$(\overline{L1})_{iv} + (\overline{L2})_{av}$	59	52	501	487	5656	5245
	$\sum_{\mu\nu M}(\mu\nu\|M)\bar{\Gamma}_{\mu\nu}^{M,\beta}$	69	59	410	367	3532	3054
Gradient III	$(\overline{L3})$	183	147	828	666	4795	3577
	Z vector	627	507	2832	2304	16 760	12 720
	$\Gamma_{\mu\nu\lambda\sigma}^{S}$	711	573	3281	2687	19 660	15 040

[a] Cutoff for integral thresholding/SCF covergence criterion. [b] CPU timing = correlation energy + SOS-MP2 gradient.

solely in the formation of the pieces of *Gradient I* as the corresponding steps in the RIMP2 gradient involve terms that are fifth-order in nature. The *Gradient II* and *Gradient III* sections are common for both OS-MP2 and RIMP2 gradient methods.

B. Chemical Tests and Application. While it is important to achieve computational speedups, we should also ensure that accuracy is not severely affected in the process. The scaled-MP2 methods, SCS-MP2, SOS-MP2, and MOS-MP2, are known to improve conventional MP2 relative energies like atomization energies, for example. Grimme et al. have also shown that the analytical SCS-MP2 gradient provides marginal statistical improvements over the MP2 geometries.[64] While this is an encouraging feature, there is no apparent computational advantage achieved by using this method. We have established in the previous sections and discussion that our OS-MP2 analytical gradient provides significant speedups relative to the RIMP2 (or SCS-MP2) analytical gradient. We will now assess the performance of the OS-MP2 analytical gradient through a statistical study of a database of main group molecules and further specific application in transition metal chemistry.

i. Statistical Study. We have recently set up a database of molecular geometries of 178 small molecules computed at various levels of theory.[41] The database consists of a variety of closed- and open-shell systems that are neutral or ionic in nature. We have used our new OS-MP2 analytical gradient techniques to obtain the structural information of these 178 molecules using two different basis sets, cc-pVDZ and cc-pVTZ.[65] Table 5 gives the statistical errors obtained relative to experimental bond lengths for various methods like conventional MP2, RIMP2, SCS-MP2, SOS-MP2, and MOS-MP2. For each basis set considered, the mean absolute deviation (MAD) and root-mean-squared (RMS) errors obtained relative to experimental data for the various flavors of MP2 are very similar. This consistency over such a diverse collection of molecules indicates that reliable geometries can be obtained from these scaled-MP2 methods. In general,

Table 5. Statistical Errors in Calculated Bond Lengths of 178 Molecules[a] Relative to Experimental Bond Lengths (r_e) in Picometers

method	MAD[b]	RMS[c]	MAX[d]
	cc-pVDZ		
MP2	2.776	3.698	16.862
RIMP2	2.767	3.691	16.864
SCSMP2	2.776	3.632	16.734
SOSMP2	2.791	3.639	16.668
MOSMP2	3.201	4.078	17.641
	cc-pVTZ		
MP2	1.403	2.172	8.237
RIMP2	1.410	2.157	8.234
SCSMP2	1.359	2.111	8.270
SOSMP2	1.361	2.121	8.286
MOSMP2	1.828	2.443	8.184

[a] See Distasio et al.[41] [b] MAD: Mean absolute deviation [c] RMS: Root mean-squared deviation [d] MAX: Maximum absolute error

MOS-MP2 appears to make a slightly larger error (off by ~0.2−0.5 pm) than the other MP2 methods. MAD and RMS are found to improve for all methods by ~1.4−1.5 pm when the size of the basis set is improved from cc-pVDZ to cc-pVTZ, which indicates the value of using the larger basis set. There is an even more significant change in the maximum absolute (MAX) error (reduced by about 50%) when changing the basis set from cc-pVDZ to cc-pVTZ. These trends indicate that the OS-MP2 methods can provide reliable geometries of molecules that are in general well-described by traditional MP2.

ii. Study of Group VI Transition Metal Carbonyl Systems. Although the scaled-MP2 methods are expected to improve the conventional MP2 picture, it is not apparent in the previous statistical study. One way to establish whether improvements are obtained is to study systems that are known to be difficult for traditional MP2. Computational TM chemistry has remained a formidable challenge to the theoretical community owing to its complex electronic structure and high computational requirements.[66,67] Over the years, DFT has proved to be the most popular methodology used to describe TM geometries and bond energies,[66−69] while conventional ab initio methods like HF and MP2 have shown limited success with the closed-shell TM complexes.[47] Higher-correlation treatments like CCSD(T) would ideally provide reliable bond energies but are limited to small systems and cannot be routinely used due to the expensive nature of such calculations. In particular, MP2 is known to consistently underestimate the metal−ligand bond distances and, thereby, overestimate the corresponding bond energies.[47] It was established recently that the closely related scaled-MP2 method, SCS-MP2, provides an improved structural description of certain transition metal compounds. Also, when the scaling idea is extended to a higher order of the MP*n* series, namely, SCS-MP3, considerable improvements are obtained in description of the thermochemistry of representative TM carbonyl compounds.[57]

To assess the performance of our analytical gradient implementation of SOS-MP2 and MOS-MP2, we have considered similar examples of TM−carbonyl complexes such as $M(CO)_6$, $M(CO)_5H_2$, and $M(CO)_3(C_6H_6)$ (M = Cr, Mo). The geometries of these complexes were optimized at the SOS-MP2 and MOS-MP2 levels. The bond dissociation energies (D_0) of the M−CO bond in $M(CO)_6$ and $M(CO)_3(C_6H_6)$ and the M−H_2 bond in $M(CO)_5H_2$ were also evaluated at the same level of theory. The Stuttgart−Bonn set[70,71] of effective core potentials (ECP) was used to describe the TM core, while the 6-311G** basis set was used for the other lighter elements, and a triple-ζ valence polarized auxiliary basis was used as a fitting basis.[72] All the methods considered predict octahedral (O_h) symmetry for the $M(CO)_6$ complexes, C_{3v} symmetry for the C_6H_6−$M(CO)_3$ systems, and C_{2v} symmetry for the $M(CO)_5(H_2)$ complexes. The SOS-MP2 optimized geometries of the Cr systems considered are shown in Figure 1. Table 6 summarizes the main structural characteristics obtained when the aforementioned systems were optimized with RIMP2 and the three scaled-MP2 theories. We have also included, for purposes of comparison, the structural features obtained from DFT optimizations using two different, popular functionals, B3LYP[73] and BP86.[74,75] Table 6 also indicates the relative error in various bond lengths (indicated within parenthesis) with respect to experimental data, if available.

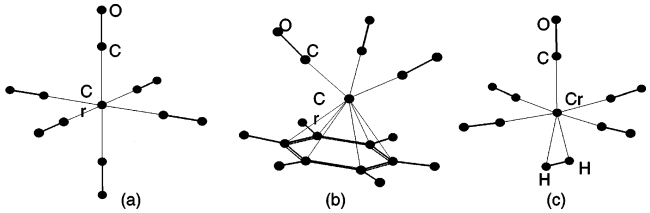

Figure 1. Obtained SOS-MP2 optimized geometries of (a) $Cr(CO)_6$, (b) C_6H_6−$Cr(CO)_3$, and (c) $Cr(CO)_5(H_2)$. For further structural details, refer to Table 6.

The data provided in Table 6 suggest that RIMP2 consistently underestimates the metal−carbonyl (M−CO) and metal−carbon(benzene) [M−C(arene)] bond distances [with the exception of Mo−CO bond length for the complex C_6H_6−$Mo(CO)_3$], consistent with previous studies. All three scaled-MP2 theories are able to correct this underestimation and predict bond distances that are closer to the experimental values. In particular, SOS-MP2 provides the best M−CO and M−C(arene) bond lengths among the various flavors of MP2, closely followed by MOS-MP2 and SCS-MP2. For example, for the complex $Cr(CO)_6$, the predicted absolute error (relative to experimental data) in the RIMP2 Cr−CO bond length is reduced from 6 to 1.9 pm by SOS-MP2, while MOS-MP2 and SCS-MP2 are off by 2.4 and 3.4 pm, respectively. The geometries predicted by DFT (both B3LYP and BP86) are consistently closer to the experimental information than the MP2 family, with BP86 providing slightly better structures than B3LYP.[69] The only exception to the trend observed is the Mo−CO bond distance in the complex C_6H_6−$Mo(CO)_3$. In this case, RIMP2 seems to predict the best Mo−CO bond length (error of 0.7 pm), while the remaining methods including the DFT results seem to overestimate the bond distance. This apparent success of RIMP2 seems fortuitous and raises doubts about the validity of the corresponding experimental data. The MP2-type methods and BP86 tend to overestimate the CO bond distances in most cases, while B3LYP tends to shorten the

Table 6. Optimized Geometrical Features (Bond Lengths) of the Group VI Transition Metal Carbonyl Complexes Obtained at the Various MP2 Levels and with the DFT Functionals Considered (in Picometers)[a]

system	experiment	RIMP2	SOS-MP2	SCS-MP2	MOS-MP2	B3LYP	BP86
			M−CO				
$Cr(CO)_6$	191.8[b]	185.8	189.9	188.4	189.4	192.1	190.4
		(−6)	(−1.9)	(−3.4)	(−2.4)	(0.3)	(−1.4)
$Mo(CO)_6$	206.3[b]	203.8	206.4	205.5	205.7	207.7	206.5
		(−2.5)	(0.1)	(−0.8)	(−0.6)	(1.4)	(0.2)
$C_6H_6-Cr(CO)_3$	184.5[c]	176.3	181.3	179.5	180.8	185.5	183.9
		(−8.2)	(−3.2)	(−5)	(−3.7)	(1)	(−0.6)
$C_6H_6-Mo(CO)_3$	196[d]	196.7	199.1	198.3	198.7	198.5	197.9
		(0.7)	(3.1)	(2.3)	(2.7)	(2.5)	(1.9)
$Cr(CO)_5(H_2)$		185.6	190.2	188.6	189.6	191.8	186.6
		179.2	183.7	182.2	183.1	191.8	190.1
$Mo(CO)_5(H_2)$		197.6	200.0	199.1	198.8	201.6	200.6
		203.3	206.0	205.1	205.3	207.2	205.9
			M−C (Arene)				
$C_6H_6-Cr(CO)_3$	223[c]	216.6	220.2	218.8	219.8	225.2	223
		(−6.4)	(−2.8)	(−4.2)	(−3.2)	(2.2)	(0)
$C_6H_6-Mo(CO)_3$	237.6[d]	230.6	233.3	232.4	232.7	240.8	238.7
		(−7.0)	(−4.3)	(−5.2)	(−4.9)	(3.2)	(1.1)
			CO				
CO	112.8[e]	113.7	113.4	113.5	113.7	112.6	113.9
		(0.9)	(0.6)	(0.7)	(0.9)	(−0.2)	(1.1)
$Cr(CO)_6$	114.1[b]	115.6	115.0	115.2	115.3	114.0	115.5
		(1.5)	(0.9)	(1.1)	(1.2)	(−0.1)	(1.4)
$Mo(CO)_6$	114.5[b]	115.3	114.8	115.0	115.2	114.0	115.4
		(0.8)	(0.3)	(0.5)	(0.7)	(−0.5)	(0.9)
$C_6H_6-Cr(CO)_3$	115.8[c]	117.4	116.3	116.6	116.8	115.2	116.7
		(1.6)	(0.5)	(0.8)	(1.0)	(−0.6)	(0.9)
$C_6H_6-Mo(CO)_3$	116.1[d]	116.3	115.8	115.9	116.2	115.3	116.7
		(0.2)	(−0.3)	(−0.2)	(0.1)	(−0.8)	(0.6)
$Cr(CO)_5(H_2)$		116.3	115.6	115.8	115.9	114.1	115.7
$Mo(CO)_5(H_2)$		115.7	115.2	115.3	115.4	114.3	115.7
			$Cr-H_2$				
$Cr(CO)_5(H_2)$		166.4	171.5	169.6	171.1	170	171.6
$Mo(CO)_5(H_2)$		186	189	188.1	189.6	192	190.3
			H−H				
H_2	74.2	73.8	73.9	73.9	74.3	74.4	75.2
		(−0.4)	(−0.3)	(−0.3)	(0.1)	(0.2)	(1.0)
$Cr(CO)_5(H_2)$		83.2	80.8	81.6	82	81.4	82.6
$Mo(CO)_5(H_2)$		81.3	80.2	80.5	80.8	79.9	81.8

[a] The deviation from available experimental data is indicated within parantheses for each indicated method. [b] References 79 and 80. [c] Reference 81. [d] Reference 82. [e] Reference 83.

C−O bond. However, the absolute magnitude of the error in the CO bond length is smaller than the M−CO and M−C(arene) cases discussed above. In particular, the deviation from the experimental CO bond distances appears to be lower for the scaled-MP2 methods, especially SOS-MP2, relative to RIMP2 and BP86. There is no experimental structural information currently available for the $M(CO)_5H_2$ systems. However, the scaled-MP2 theories continue to predict bond lengths [M−CO, M−C(arene), and CO] that are slightly longer than the RIMP2 case, consistent with the trend discussed above.

Table 7 summarizes the theoretical bond dissociation energies (D_0) obtained using the aforementioned methods. The D_0 values are obtained by correcting the electronic dissociation energy (D_e) for changes in the zero-point vibrational energies. Subsequent thermodynamic corrections arising from the translational, vibrational, and rotational degrees of freedom, as well as pV work (assuming ideal behavior), were determined to be <2 kcal/mol for the systems considered here. This information was obtained from the vibrational frequency analysis performed on the optimized structure at each level of theory considered above. Due to the lack of analytical second derivatives for the RIMP2, SOS-MP2, SCS-MP2, and MOS-MP2 methods, the vibrational frequencies were obtained by performing numerical differentiation of the respective analytical gradients. We also note here that the calculated electronic dissociation energies have not been corrected for basis set superposition error on the basis of previous recommendations.[47] To further substantiate the calculated dissociation energies, we have also

Table 7. Calculated Bond Dissociation Energies, Namely M−CO and M−H_2, of the Various Group VI Transition Metal Carbonyls Considered at Different Levels of MP2 Theory, DFT and CCSD(T) (in kcal/mol)

system	exptl	RIMP2	SOS-MP2	SCS-MP2	MOS-MP2	B3LYP	BP86	CCSD(T)[a]
$Cr(CO)_6$	36.80[b]	56.62	44.04	48.35	48.45	34.87	41.07	41.71
	e_1[c]	(19.82)	(7.24)	(11.55)	(11.65)	(−1.93)	(4.27)	
	e_2[d]	*14.91*	*2.33*	*6.64*	*6.74*	*−6.84*	*−0.64*	
$Mo(CO)_6$	40.50[b]	46.45	38.87	41.46	41.82	38.15	41.13	39.58
	e_1[c]	(5.95)	(−1.63)	(0.96)	(1.32)	(−2.35)	(0.63)	
	e_2[d]	*6.87*	*−0.72*	*1.88*	*2.24*	*−1.43*	*1.54*	
C_6H_6−$Cr(CO)_3$	51.89[e]	74.90	54.39	60.98	60.29	43.20	51.93	
C_6H_6−$Mo(CO)_3$		60.33	49.40	53.01	54.07	49.88	55.59	
$Cr(CO)_5(H_2)$	15.00[f]	24.69	17.51	19.95	20.14	11.44	16.51	17.64
	e_1[c]	(9.69)	(2.51)	(4.95)	(5.14)	(−3.56)	(1.51)	
	e_2[d]	*7.05*	*−0.13*	*2.31*	*2.50*	*−6.20*	*−1.13*	
$Mo(CO)_5(H_2)$		17.81	13.81	15.12	15.82	11.05	12.48	15.16
	e_2[d]	*2.65*	*−1.35*	*−0.04*	*0.66*	*−4.12*	*−2.68*	

[a] CCSD(T) calculation performed on the BP86 optimized geometry. [b] Reference 84. [c] e_1: error relative to experiment (indicated method − expt). [d] e_2: error relative to CCSD(T) [indicated method − CCSD(T)]. [e] DFT estimates from refs 77 and 78. [f] Reference 85.

performed the highly accurate CCSD(T) calculations on the BP86 optimized geometry using the same ECP and basis set as before. Due to the expensive nature of this method, we have been limited to the smaller systems, $M(CO)_6$ and $M(CO)_5(H_2)$. Table 7 also provides information about the relative errors (e_1) between the calculated D_0 value and available experimental data (numbers indicated within parentheses).

The relative errors (e_1) indicate that RIMP2 tends to overestimate the M−CO and M−H_2 dissociation energies. This is consistent with the trend that RIMP2 tends to underestimate the M−CO bond length. The overestimation is significantly higher for $Cr(CO)_6$ and $Cr(CO)_5(H_2)$ with the e_1 being as high as 19.8 kcal/mol and 9.7 kcal/mol, respectively, while $Mo(CO)_6$ is about 6 kcal/mol off. This trend is consistent with the previous studies on these compounds.[68] All the scaled-MP2 methods predict D_0 values that are closer to the experimental values than RIMP2, consistent with the corresponding prediction of longer M−CO and M−H_2 bond distances. The Mo−CO bond energy in the complex $Mo(CO)_6$ is the only case where SOS-MP2 seems to underestimate the bond energy by about 2 kcal/mol, while SCS-MP2 and MOS-MP2 are about 4−5 kcal/mol better than the RIMP2 result. In general, the SCS-MP2 and MOS-MP2 results are similar in magnitude, while SOS-MP2 is sometimes better than the former results or of comparable quality. Among the DFT methods, B3LYP tends to underestimate the bond energy while BP86 consistently provides better results.[69]

The analysis so far assumes that the reference experimental values are the best available estimates of bond energies. This is not necessarily true; for example, inconsistencies between experimental and theoretical results for the Cr−(CO) first bond dissociation energy have raised doubts about the validity of the reported experimental value of 36.8 kcal/mol.[47,76] Indeed, the more reliable CCSD(T) method computed in this study with a triple-ζ-quality basis predicts a dissociation energy of about 41.7 kcal/mol and is almost 5 kcal/mol higher than the experimental estimate.[47] Also, the scaled-MP2 methods are designed to produce QCISD(T)- or CCSD(T)-quality results. Therefore, in order to make a fair comparison, we have also included the errors (e_2) obtained relative to CCSD(T) energies (italicized numbers in Table 7).

The e_2 errors are either lower than or similar to the obtained e_1 errors, indicating that the dissociation energies obtained with the scaled-MP2 methods are closer to the CCSD(T) values. In particular, the calculated SOS-MP2 bond dissociation energy for $Mo(CO)_6$ is about 0.7 kcal/mol lower than the corresponding CCSD(T) value. The corresponding e_1 error indicated that SOS-MP2 underestimated the experimental result. For the $Mo(CO)_5(H_2)$ complex, there is no experimental M−H_2 bond energy data available. However, our CCSD(T) result indicates that the trend of RIMP2 overestimation of bond energies and improvements from the scaled-MP2 methods is still valid. Also, we should note here that, with the newly proposed SOS-MP2 and MOS-MP2 analytical gradients, you can obtain these CCSD(T)-quality energies for far lower computational cost. For example, the complete geometry optimization procedure at the SOS-MP2 level for $Cr(CO)_6$ took about 2.3 h on a Linux Opteron processor, while the single-point energy evaluation performed on the same processor at the CCSD(T) level alone took about 27.3 h.

For the C_6H_6−$M(CO)_3$ systems, we are not aware of any gas-phase experimental data available on the first dissociation energy of the M−CO bond, and these systems are computationally too big to get CCSD(T) energies. Previous DFT studies on the neutral C_6H_6−$Cr(CO)_3$ system estimate the first Cr−CO bond energy to be about 52 kcal/mol.[77,78] SOS-MP2 estimates the Cr−CO bond energy to be about 54.3 kcal/mol, while SCS-MP2 and MOS-MP2 estimate about 60 kcal/mol. RIMP2 gives a much higher bond energy of 74.9 kcal/mol, while B3LYP predicts a low 43 kcal/mol. The BP86 functional predicts the bond energy to be ∼52 kcal/mol, which is in agreement with previous studies.[77,78] A similar trend is observed with the Mo analogue. These numbers are consistent with the previous discussion on the Cr−CO bond distance where RIMP2 geometry predicted a relatively short Cr−CO bond distance, while the scaled-MP2 methods are about 3−5 pm longer than RIMP2 bond distance.

V. Conclusions

In this paper, we have presented the derivation and efficient implementation of the fourth-order scaling analytical gradients of the SOS-MP2 and MOS-MP2 energies that are obtained through a combination of auxiliary basis expansions and a Laplace transformation. The theory is interesting because all fifth-order steps that arise in a conventional derivation of the opposite-spin MP2 gradient involve either four-center two-electron integrals or the pair correlation amplitudes. The former are obviously re-expressed in terms of two- and three-center quantities with the use of auxiliary basis expansions, and this paper shows that the amplitudes also likewise need never explicitly enter the gradient expressions. Instead, more compact two- and three-center intermediates in the auxiliary basis are used.

Significant computational speedups can be achieved by using these OS-MP2 analytical gradients to optimize the molecular geometry of large-sized systems. The inherent fourth-order nature of the algorithm helps to push the boundary of the size of systems currently feasible with conventional MP2 and RIMP2 methods, using reasonably sized basis sets. The largest calculation performed in this paper is the force calculation of the globular hexadeca alanine polypeptide with 1610 basis functions. The overall SOS-MP2 and MOS-MP2 force evaluation is about 3.4 times faster than the corresponding RIMP2 calculation.

Apart from the computational advantages, the OS-MP2 methods achieve either a MP2 level of accuracy or even help to improve the MP2 picture. Statistical results of the bond lengths obtained from 178 molecules indicate that the geometries obtained by the OS-MP2 methods are as good as MP2. The geometrical optimizations and subsequent calculation of the bond dissociation energies of the group VI transition metal carbonyl complexes indicate that SOS-MP2 and MOS-MP2 geometries help to significantly improve the underestimation seen in MP2 bond lengths and consequently predict M−CO and M−H_2 bond dissociation energies that are closer to experimental and CCSD(T) results.

However, one should keep in mind that methods like SOS-MP2 provide improvements in relative energies only when MP2 is known to overestimate the corresponding energy relative to higher-correlation treatments like CCSD(T).[52] Also, given the empirical nature of these OS-MP2 methods, one should probably investigate the choice of optimal parameter while studying specific properties even though in our study the recommended parameters perform just fine. Apart from these caveats, the reduced scaling OS-MP2 gradient algorithm seems to be a fast, efficient, and accurate method that can be used to determine molecular geometries of medium- to large-sized systems.

Acknowledgment. This work was supported by the Office of Basic Energy Sciences of the U.S. Department of Energy through the Computational Nanoscience Initiative, with additional support from Q-Chem Inc. through a subcontract from the NIH SBIR award 5R44GM066484-02. R.C.L. would like to thank R. P. Steele for providing the database of 178 molecules for this study. M.H.G. is a part-owner of Q-Chem Inc.

Appendix A

Outline of Steps Leading to eq 15. Direct differentiation of eqs 7 and 12 leads to

$$[{}^{\tau}X_{KL}{}^{\alpha}]^x = 2\sum_{ia}^{\alpha}[B_{ia}^K]^x B_{ia}^L({}^{\tau}\xi_i^a)^2 + t_\tau \sum_{ia}^{\alpha} B_{ia}^K B_{ia}^L({}^{\tau}\xi_i^a)^2[\epsilon_i^x - \epsilon_a^x] \tag{A1}$$

$$[B_{ia}^K]^x = \sum_M (ia|M)^x V_{MK}^{-1/2} + \sum_M (ia|M)[V_{MK}^{-1/2}]^x \tag{A2}$$

$$[V_{MK}^{-1/2}]^x = -\frac{1}{2}\sum_{NP} V_{MN}^{-1} V_{NP}^x V_{PK}^{-1/2} \tag{A3}$$

Plugging eq A3 into eq A2 would then give

$$[B_{ia}^K]^x = \sum_M (ia|M)^x V_{MK}^{-1/2} - \frac{1}{2}\sum_{PQN} B_{\mathrm{ia}}^Q V_{QN}^{-1/2} V_{NP}^x V_{PK}^{-1/2} \tag{A4}$$

When the above equation is inserted into eq A1, we get

$$[{}^{\tau}X_{KL}^{\alpha}]^x = 2\sum_{ia}^{\alpha}\sum_M (ia|M)^x V_{MK}^{-1/2} B_{ia}^L({}^{\tau}\xi_i^a)^2 - \sum_{PQN} {}^{\tau}X_{LQ}^{\alpha} V_{QN}^{-1/2} V_{NP}^x V_{PK}^{-1/2} + t_\tau \sum_{ia}^{\alpha} B_{ia}^K B_{ia}^L({}^{\tau}\xi_i^a)^2[\epsilon_i^x - \epsilon_a^x] \tag{A5}$$

Subsequently, the above equation can be incorporated into eq 14 to arrive at eq 15 by introducing the terms described by eqs 16−19 and rearranging indices appropriately.

Appendix B

Summary of the Restricted Closed-Shell Coupled-Perturbed Hartree−Fock and Related Equations.[2,37] The occupied−occupied and virtual−virtual orbital responses can be written in terms of the virtual−occupied response, orbital energy and derivatives of the overlap, one-particle Hamiltonian, and four-center two-electron integrals as shown below:

$$U_{pq}^x = \frac{Q_{pq}^x}{(\epsilon_q - \epsilon_p)} \tag{B1}$$

$$Q_{pq}^x \equiv \mathscr{B}_{pq}^x + \sum_c^{\mathrm{vir}}\sum_k^{\mathrm{occ}} A_{pqck} U_{ck}^x \tag{B2}$$

$$A_{pqrs} = 2(pq|rs) - (pr|qs) - (ps|qr) \tag{B3}$$

$$\mathscr{B}_{pq}^x = F_{pq}^{(x)} - S_{pq}^{(x)}\epsilon_q - \frac{1}{2}\sum_{kl}^{\mathrm{occ}} A_{pqlk} S_{kl}^x \tag{B4}$$

$$F_{pq}^{(x)} = H_{pq}^{(x)} + \sum_k^{\mathrm{occ}} [(pq|kk)^{(x)} - (pk|qk)^{(x)}] \tag{B5}$$

$$\epsilon_p^x = Q_{pp}^x \tag{B6}$$

The closed-shell coupled-perturbed Hartree−Fock equation in matrix notation is given by

$$\mathbf{A'U}^x = \mathscr{B}^x \tag{B7}$$

where

$$A'_{aibj} = \delta_{ab}\delta_{ij}(\epsilon_i - \epsilon_a) - A_{aibj} \tag{B8}$$

The explicit assembly of the virtual−occupied orbital responses $\mathbf{U}^x$ in eq B7 can be avoided by using the **Z**-vector method[27]

$$(\mathbf{A'})^{\mathbf{T}}\mathbf{Z} = \mathbf{L} \tag{B9}$$

where **L** is the effective Lagrangian and the **Z**-vector solution of the above equation corresponds to the virtual−occupied block of the 1-PDM $\bar{P}_{ai}$.

Appendix C

Details of the Algebraic Steps Leading to eq 26. The strategies used follow closely with that of refs 37 and 41. Expanding the summation, $\sum_p^{\text{all}} = \sum_k^{\text{occ}_\alpha} + \sum_c^{\text{vir}_\alpha} + \sum_l^{\text{occ}_\beta} + \sum_d^{\text{vir}_\beta}$, the sum of the second terms in eqs 15 and 22 can be written as

$$\sum_\tau^{N_\tau} w_\tau \sum_{ia}^{\alpha}\sum_M \{2\sum_p^{\text{all}} (pa|M)U_{pi}^x + t_\tau(ia|M)\epsilon_i^x\}{}^\tau\Gamma_{ia}^{M,\beta}({}^\tau\xi_i^a)^2 =$$
$$\sum_\tau^{N_\tau} w_\tau \sum_{ia}^{\alpha}\sum_M \{2\sum_k^{\alpha} (ka|M)U_{ki}^x +$$
$$2\sum_c^{\alpha} (ca|M)U_{ci}^x + t_\tau(ia|M)\epsilon_i^x\}{}^\tau\Gamma_{ia}^{M,\beta}({}^\tau\xi_i^a)^2 \tag{C1}$$

When the spin orthonormality constraint in eq 25 is used, the first term in the above equation can be rewritten as

$$2\sum_\tau^{N_\tau} w_\tau \sum_{ika}^{\alpha}\sum_M (ka|M)U_{ki}^x\,{}^\tau\Gamma_{ia}^{M,\beta}({}^\tau\xi_i^a)^2 =$$
$$\sum_\tau^{N_\tau} w_\tau \sum_{ika}^{\alpha}\sum_{KL} (U_{ki}^x - U_{ik}^x)B_{ka}^K B_{ia}^L\,{}^\tau X_{KL}^\beta({}^\tau\xi_i^a)^2 -$$
$$\sum_\tau^{N_\tau} w_\tau \sum_{ika}^{\alpha}\sum_M S_{ki}^x(ka|M){}^\tau\Gamma_{ia}^{M,\beta}({}^\tau\xi_i^a)^2 \tag{C2}$$

As the indicies, *k* and *i*, both span over the same set of occupied α orbitals, the summation over these indicies can be expanded as $\sum_{ki}^{\alpha} = \sum_{k>i}^{\alpha} + \sum_{k<i}^{\alpha} + \sum_{k=i}^{\alpha}$. When this expansion is used and the indicies *k* and *i* are exchanged for the second term, eq C2 can then be written as

$$= \sum_\tau^{N_\tau} w_\tau \sum_a^{\alpha}\sum_{KL}\sum_{k>i}^{\alpha} (U_{ki}^x - U_{ik}^x)B_{ka}^K B_{ia}^L X_{KL}^\beta[(\xi_i^a)^2 - (\xi_k^a)^2] -$$
$$\sum_{ki}^{\alpha} \overline{(L1)}_{ki} S_{ki}^x \tag{C3}$$

We now introduce a function, ${}^\tau g_{ki}$, defined by eq 29 and further use eq B1 to express the above equation as

$$= \sum_\tau^{N_\tau} w_\tau \sum_a^{\alpha}\sum_{KL}\sum_{k>i}^{\alpha} (Q_{ki}^x + Q_{ik}^x)B_{ka}^K B_{ia}^L\,{}^\tau X_{KL}^\beta({}^\tau\xi_i^a)^2\,{}^\tau g_{ki} -$$
$$\sum_{ki}^{\alpha} \overline{(L1)}_{ki} S_{ki}^x \tag{C4}$$

In the above equation, the energy denominator in eq B1 is effectively removed with the introduction of the function, ${}^\tau g_{ki}$, thereby neatly avoiding the potential singularity problem that would arise when nearly degenerate orbitals are encountered. Also, the function, ${}^\tau g_{ki}$, is continuous when $\epsilon_i \approx \epsilon_k$. The last term in eq C1 can be written in terms of the ${}^\tau g_{ki}$ function as

$$\sum_\tau^{N_\tau} w_\tau t_\tau \sum_{ia}^{\alpha}\sum_M (ia|M){}^\tau\Gamma_{ia}^{M,\beta}({}^\tau\xi_i^a)^2\epsilon_i^x =$$
$$\sum_\tau^{N_\tau} w_\tau \sum_{KL}\sum_{ia}^{\alpha} B_{ia}^K B_{ia}^L\,{}^\tau X_{KL}^\beta({}^\tau\xi_i^a)^2\,{}^\tau g_{ii} Q_{ii}^x \tag{C5}$$

Combining eqs C4 and C5, and using the inverse of the mathematical summation trick used to arrive at eq C3, we can easily write the sum of the terms considered in eq C1 as eq 26.

References

(1) Pulay, P. *Mol. Phys.* **1969**, *17*, 197.

(2) Yamaguchi, Y.; Osamura, Y.; Goddard, J. D.; Schaefer, H. F., III. *A New Dimension to Quantum Chemistry: Analytic Derivative Methods in ab Initio Molecular Electronic Structure Theor*; Oxford University Press: New York, 1994.

(3) Parr, R. G.; Yang, W. *Density-Functional Theory of Atoms and Molecules*; Oxford: New York, 1989.

(4) Kristyan, S.; Pulay, P. *Chem. Phys. Lett.* **1994**, *229*, 175−180.

(5) Cerny, J.; Hobza, P. *Phys. Chem. Chem. Phys.* **2005**, *7*, 1624−1626.

(6) Tsuzuki, S.; Luthi, H. P. *J. Chem. Phys.* **2001**, *114*, 3949−3957.

(7) van Mourik, T.; Gdanitz, R. J. *J. Chem. Phys.* **2002**, *116*, 9620−9623.

(8) Beachy, M. D.; Chasman, D.; Murphy, R. B.; Halgren, T. A.; Friesner, R. A. *J. Am. Chem. Soc.* **1997**, *119*, 5908−5920.

(9) Møller, C.; Plesset, M. S. *Phys. Rev.* **1934**, *46*, 618−622.

(10) Szabo, A.; Ostlund, N. S. *Modern Quantum Chemistry: Introduction to Advanced Electronic Structure Theory*; Dover Publications, Inc.: New York, 1996.

(11) Mourik, T. V.; Wilson, A. K.; Dunning, T. H. *Mol. Phys.* **1999**, *96*, 529−547.

(12) Feyereisen, M.; Fitzgerald, G.; Komornicki, A. *Chem. Phys. Lett.* **1993**, *208*, 359−363.

(13) Saebo, S.; Pulay, P. *Ann. Rev. Phys. Chem.* **1993**, *44*, 213−236.

(14) Weigend, F.; Haser, M.; Patzelt, H.; Ahlrichs, R. *Chem. Phys. Lett.* **1998**, *294*, 143.

(15) Schütz, M.; Hetzer, G.; Werner, H. J. *J. Chem. Phys.* **1999**, *111*, 5691−5705.

(16) Ayala, P. Y.; Scuseria, G. E. *J. Chem. Phys.* **1999**, *110*, 3660−3671.

(17) Hetzer, G.; Schütz, M.; Stoll, H. *J. Chem. Phys.* **2000**, *113*, 9443−9455.

(18) Lee, M. S.; Maslen, P. E.; Head-Gordon, M. *J. Chem. Phys.* **2000**, *112*, 3592−3601.

(19) Pulay, P.; Saebo, S.; Wolinski, K. *Chem. Phys. Lett.* **2001**, *344*, 543−552.

(20) Ayala, P. Y.; Kudin, K. N.; Scuseria, G. E. *J. Chem. Phys.* **2001**, *115*, 9698−9707.

(21) Saebo, S.; Pulay, P. *J. Chem. Phys.* **2001**, *115*, 3975−3983.

(22) Werner, H. J.; Manby, F. R.; Knowles, P. J. *J. Chem. Phys.* **2003**, *118*, 8149−8160.

(23) DiStasio, R. A.; Jung, Y. S.; Head-Gordon, M. *J. Chem. Theory Comput.* **2005**, *1*, 862−876.

(24) Subotnik, J. E.; Head-Gordon, M. *J. Chem. Phys.* **2005**, *122*, 034109.

(25) Haser, M. *Theor. Chim. Acta* **1993**, *87*, 147−173.

(26) Pople, J. A.; Krishnan, R.; Schelgel, H. B.; Binkley, J. S. *Int. J. Quantum Chem. Symp.* **1979**, *13*, 225.

(27) Handy, N. C.; Schaefer, H. F. *J. Chem. Phys.* **1984**, *81*, 5031−5033.

(28) Handy, N. C.; Amos, R. D.; Gaw, J. F.; Rice, J. E.; Simandiras, E. D. *Chem. Phys. Lett.* **1985**, *120*, 151−158.

(29) Helgaker, T.; Jorgensen, P.; Handy, N. C. *Theor. Chim. Acta* **1989**, *76*, 227−245.

(30) Frisch, M. J.; Headgordon, M.; Pople, J. A. *Chem. Phys. Lett.* **1990**, *166*, 275−280.

(31) Frisch, M. J.; Headgordon, M.; Pople, J. A. *Chem. Phys. Lett.* **1990**, *166*, 281−289.

(32) Haase, F.; Ahlrichs, R. *J. Comput. Chem.* **1993**, *14*, 907−912.

(33) Nielsen, I. M. B. *Chem. Phys. Lett.* **1996**, *255*, 210−216.

(34) Fletcher, G. D.; Rendell, A. P.; Sherwood, P. *Mol. Phys.* **1997**, *91*, 431−438.

(35) El Azhary, A.; Rauhut, G.; Pulay, P.; Werner, H. J. *J. Chem. Phys.* **1998**, *108*, 5185−5193.

(36) Head-Gordon, M. *Mol. Phys* **1999**, *96*, 673−679.

(37) Aikens, C. M.; Webb, S. P.; Bell, R. L.; Fletcher, G. D.; Schmidt, M. W.; Gordon, M. S. *Theor. Chem. Acc.* **2003**, *110*, 233−253.

(38) Gerenkamp, M.; Grimme, S. *Chem. Phys. Lett.* **2004**, *392*, 229−235.

(39) Saebo, S.; Baker, J.; Wolinski, K.; Pulay, P. *J. Chem. Phys.* **2004**, *120*, 11423−11431.

(40) Rhee, Y. M.; DiStasio, R. A.; Lochan, R. C.; Head-Gordon, M. *Chem. Phys. Lett.* **2006**, *426*, 197−203.

(41) DiStasio, R. A.; Steele, R. P.; Rhee, Y. M.; Shao, Y.; Head-Gordon, M. *J. Comput. Chem.* **2007**, *28*, 839−856.

(42) Weigend, F.; Haser, M. *Theor. Chem. Acc.* **1997**, *97*, 331−340.

(43) Schütz, M.; Werner, H. J.; Lindh, R.; Manby, F. R. *J. Chem. Phys.* **2004**, *121*, 737−750.

(44) Helgaker, T.; Gauss, J.; Jorgensen, P.; Olsen, J. *J. Chem. Phys.* **1997**, *106*, 6430−6440.

(45) Raghavachari, K.; Trucks, G. W.; Pople, J. A.; Head-Gordon, M. *Chem. Phys. Lett.* **1989**, *157*, 479−483.

(46) Sinnokrot, M. O.; Sherrill, C. D. *J. Phys. Chem. A* **2004**, *108*, 10200−10207.

(47) Frenking, G.; Antes, I.; Böhme, M.; Dapprich, S.; Ehlers, A. W.; Jonas, V.; Neuhaus, A.; Otto, M.; Stegmann, R.; Veldkamp, A.; Vyboishchikov, S. F. Pseudopotential Calculations of Transition Metal Compunds: Scope and Limitations. In *Reviews in Computational Chemistry*, Lipkowitz, K. B., Boyd, D. B., Eds.; VCH Publishers, Inc.: New York, 1996; Vol. 8.

(48) Byrd, E. F. C.; Sherrill, C. D.; Head-Gordon, M. *J. Phys. Chem. A* **2001**, *105*, 9736−9747.

(49) Helgaker, T.; Klopper, W.; Koch, H.; Noga, J. *J. Chem. Phys.* **1997**, *106*, 9639−9646.

(50) Grimme, S. *J. Chem. Phys.* **2003**, *118*, 9095−9102.

(51) Jung, Y.; Lochan, R. C.; Dutoi, A. D.; Head-Gordon, M. *J. Chem. Phys.* **2004**, *121*, 9793−9802.

(52) Lochan, R. C.; Jung, Y.; Head-Gordon, M. *J. Phys. Chem. A* **2005**, *109*, 7598−7605.

(53) Goumans, T. P. M.; Ehlers, A. W.; Lammertsma, K.; Wurthwein, E. U.; Grimme, S. *Chem.—Eur. J.* **2004**, *10*, 6468−6475.

(54) Grimme, S. *Chem.—Eur. J.* **2004**, *10*, 3423−3429.

(55) Grimme, S. *J. Phys. Chem. A* **2005**, *109*, 3067−3077.

(56) Grimme, S.; Muck-Lichtenfeld, C.; Wurthwein, E. U.; Ehlers, A. W.; Goumans, T. P. M.; Lammertsma, K. *J. Phys. Chem. A* **2006**, *110*, 2583−2586.

(57) Hyla-Kryspin, I.; Grimme, S. *Organometallics* **2004**, *23*, 5581−5592.

(58) Dunlap, B. I. *Phys. Chem. Chem. Phys.* **2002**, *2*, 2113−2116.

(59) Almlöf, J. *Chem. Phys. Lett.* **1991**, *181*, 319−320.

(60) Jung, Y.; Head-Gordon, M. *Phys. Chem. Chem. Phys.* **2006**, *8*, 2831−2840.

(61) Rice, J. E.; Amos, R. D. *Chem. Phys. Lett.* **1985**, *122*, 585−590.

(62) Head-Gordon, M.; Maslen, P. E.; White, C. A. *J. Chem. Phys.* **1998**, *108*, 616−625.

(63) Shao, Y.; Molnar, L. F.; Jung, Y.; Kussmann, J.; Ochsenfeld, C.; Brown, S. T.; Gilbert, A. T. B.; Slipchenko, L. V.; Levchenko, S. V.; O'Neill, D. P.; DiStasio, R. A.; Lochan, R. C.; Wang, T.; Beran, G. J. O.; Besley, N. A.; Herbert, J. M.; Lin, C. Y.; Van Voorhis, T.; Chien, S. H.; Sodt, A.; Steele, R. P.; Rassolov, V. A.; Maslen, P. E.; Korambath, P. P.; Adamson, R. D.; Austin, B.; Baker, J.; Byrd, E. F. C.; Dachsel, H.; Doerksen, R. J.; Dreuw, A.; Dunietz, B. D.; Dutoi, A. D.; Furlani, T. R.; Gwaltney, S. R.; Heyden, A.; Hirata, S.; Hsu, C. P.; Kedziora, G.; Khalliulin, R. Z.; Klunzinger, P.; Lee, A. M.; Lee, M. S.; Liang, W.; Lotan, I.; Nair, N.; Peters, B.; Proynov, E. I.; Pieniazek, P. A.; Rhee, Y. M.; Ritchie, J.; Rosta, E.; Sherrill, C. D.; Simmonett, A. C.; Subotnik, J. E.; Woodcock, H. L.; Zhang, W.; Bell, A. T.; Chakraborty, A. K.; Chipman, D. M.; Keil, F. J.; Warshel, A.; Hehre, W. J.; Schaefer, H. F.; Kong, J.; Krylov, A. I.; Gill, P. M. W.; Head-Gordon, M. *Phys. Chem. Chem. Phys.* **2006**, *8*, 3172−3191.

(64) Gerenkamp, M.; Grimme, S. *Chem. Phys. Lett.* **2004**, *392*, 229−235.

(65) Kendall, R. A.; Dunning, T. H., Jr.; Harris, R. J. *J. Chem. Phys.* **1992**, *96*, 6796−6806.

(66) Frenking, G.; Wagener, T. *Encyclopedia of Computational Chemistry*; Wiley: New York, 1998; pp 3073−3084.

(67) Veillard, A. *Chem. Rev.* **1991**, *91*, 743−766.

(68) Ziegler, T. *Chem. Rev.* **1991**, *91*, 651−667.

(69) Furche, F.; Perdew, J. P. *J. Chem. Phys.* **2006**, *124*, 044103.

(70) Andrae, D.; Haussermann, U.; Dolg, M.; Stoll, H.; Preuss, H. *Theor. Chim. Acta* **1990**, *77*, 123−141.

(71) Dolg, M.; Wedig, U.; Stoll, H.; Preuss, H. *J. Chem. Phys.* **1987**, *86*, 2123−2131.

(72) Weigend, F.; Haser, M.; Patzelt, H.; Ahlrichs, R. *Chem. Phys. Lett.* **1998**, *294*, 143−152.

(73) Becke, A. D. *J. Chem. Phys.* **1993**, *98*, 1372−1377.

(74) Becke, A. D. *Phys. Rev. A: At., Mol., Opt. Phys.* **1988**, *38*, 3098−3100.

(75) Perdew, J. P. *Phys. Rev. B: Condens. Matter Mater. Phys.* **1986**, *33*, 8822−8824.

(76) Li, J.; Schreckenbach, G.; Ziegler, T. *J. Phys. Chem.* **1994**, *98*, 4838−4841.

(77) Li, Y.; McGrady, J. E.; Baer, T. *J. Am. Chem. Soc.* **2002**, *124*, 4487−4494.

(78) McGrady, J. E.; Dyson, P. J. *J. Organomet. Chem.* **2000**, *607*, 203−207.

(79) Arnesen, S. P.; Seip, H. M. *Acta Chem. Scand.* **1966**, *20*, 2711.

(80) Jost, A.; Rees, B.; Yelon, W. B. *Acta Crystallogr., Sect. B: Struct. Sci.* **1975**, *31*, 2649−2658.

(81) Rees, B.; Coppens, P. *Acta Crystallogr., Sect. B: Struct. Sci.* **1973**, *29*, 2516−2528.

(82) Burgi, H. B.; Raselli, A.; Braga, D.; Grepioni, F. *Acta Crystallogr., Sect. B: Struct. Sci.* **1992**, *48*, 428−437.

(83) Huber, K. P.; Herzberg, G. *Molecular Spectra and Molecular Structure. IV. Constants of Diatomic Molecules;* Van Nostrand Reinhold Co.: New York, 1979.

(84) Lewis, K. E.; Golden, D. M.; Smith, G. P. *J. Am. Chem. Soc.* **1984**, *106*, 3905−3912.

(85) Wells, J. R.; House, P. G.; Weitz, E. *J. Phys. Chem.* **1994**, *98*, 8343−8351.

CT600292H